Spatially Multiplexed Single-molecule Translocations through a Nanopore at Controlled Speeds

S. M. Leitao[1], V. Navikas[2], H. Miljkovic[2], B. Drake[1], S. Marion[2], G. Pistoletti Blanchet[3], K. Chen[4], S. F. Mayer[2], U. F. Keyser[4], A. Kuhn[3], G. E. Fantner[1]* and A. Radenovic[2]*

*corresponding authors

[1]*Laboratory for Bio- and Nano-Instrumentation, Institute of Bioengineering, School of Engineering, EPFL, 1015, Lausanne, Switzerland*

[2]*Laboratory of Nanoscale Biology, Institute of Bioengineering, School of Engineering, EPFL, 1015, Lausanne, Switzerland*

[3]*HES-SO Valais-Wallis - Haute Ecole d'Ingénierie, 1950, Sion, Switzerland*

[4]*Cavendish Laboratory, University of Cambridge, CB3 0HE, Cambridge, United Kingdom*

List of the corresponding authors:

Aleksandra Radenovic, aleksandra.radenovic@epfl.ch

Georg Fantner, georg.fantner@epfl.ch

Abstract

In current nanopore-based label-free single-molecule sensing technologies, stochastic processes influence the selection of the translocating molecule, translocation rate and translocation velocity. As a result, single-molecule translocations are challenging to control spatially and temporally. Here we present a method using a glass nanopore mounted on a 3D nanopositioner to spatially select molecules, deterministically tethered on a glass surface, for controlled translocations. By controlling the distance between the nanopore and the glass surface, we can actively select the region of interest on the molecule and scan it a controlled number of times and at a controlled velocity. Decreasing the velocity and averaging thousands of consecutive readings of the same molecule increases the signal-to-noise ratio (SNR) by two orders of magnitude compared to free translocations. We demonstrate the method's versatility by assessing DNA-protein complexes, DNA rulers and DNA gaps achieving down to single nucleotide gap detection.

Biological nanopores have been used to successfully sequence single-stranded DNA (ssDNA) and peptides which is made possible by slowing the speed of the translocation with protein motors[1-5]. However, the stochastic nature of which molecule enters the pore at which time, as well as the residual fluctuation in the feed rate of the protein motor remains challenging[6].

Solid-state nanopores have been engineered to attempt the same molecular detectability of biological nanopores while keeping full control of the pore design and properties in a stable system[7–11]. Pores can be tuned to the desired size for the molecules in question, enabling the detection and characterization of a broad range of biomolecules such as double-stranded DNA (dsDNA), proteins and DNA-protein complexes[11,12]. However, speed control with molecular motors has not yet been demonstrated with solid-state nanopores. Even though the conductance drop in solid-state nanopores can be higher than in biological nanopores, the uncontrolled translocation speed hampers the potentially higher SNR[13,14]. Therefore, the free translocation speed limits high fidelity measurements, making single base pair resolution along freely translocating dsDNA challanging to achieve.

Uncontrolled velocity limits the temporal and spatial resolution due to a finite amplifier bandwidth and the noise density integrated over the measurement bandwidth[15]. This limitation decreases the signal-to-noise ratio (SNR), critical for detecting small features along the DNA nanostructure[6]. High translocation speeds and low SNR on single readings have thus far hampered the use of solid-state devices in the study of complex forms of dsDNA.

Nanocapillaries, referred to as glass nanopores, are well suited for the detection of DNA structures[16,17] since they have good SNR characteristics for high-bandwidth measurements. Glass nanopores can be manufactured to radii below 10 nm by precisely controlling the diameter of the

opening with an electron beam irradiation or by depositing the additional coatings by controllable wet-chemical silanization[18]. They can also be integrated with other techniques, such as optical detection, atomic force microscopy (AFM)[19,20] and optical tweezers[21]. The latter allows probing force during translocation, but the very high force resolution requires low optical trap stiffness and prevents sub-nanometer displacement control.

Scanning Ion Conductance Microscopy (SICM), on the other hand has very high accuracy displacement control combined with high-bandwidth, low-noise current sensing. SICM uses a glass nanopore as a probe to image biological surfaces by moving the nanocapillary with nanometer precision towards a surface while measuring the current to detect the sample topography[22–24]. This microscopy method reveals the dynamics of nanostructures on the cell membrane and can be combined with super-resolution fluorescence techniques[25,26]. Here we utilize the benefits of SICM to overcome the limitations of uncontrolled translocation of DNA through glass nanopores by combining the high SNR and high bandwidth of the glass nanopores with the high degree of displacement control of SICM to achieve accurate, repeated control of single-molecule translocation experiments.

Single-molecule translocations controlled by Nanopositioner

We modified our previously developed high-speed scanning ion conductance microscope (HS-SICM) setup[25] with a closed loop, long-range XYZ piezo scanner to accurately control the pipette motion and perform controlled translocations of spatially multiplexed molecules (Figure 1a). Analogously to single-molecule force spectroscopy experiments[27] performed by AFM that generate force-distance traces, with SICM, we generate conductance-distance traces of single molecules. We, therefore, refer to our measurements as scanning ion conductance spectroscopy

(SICS), a nanopore-based method for controlled translocations. To demonstrate the principle of a controlled translocation with SICS, we used a DNA-dCas9 construct to generate a conductance-distance fingerprint of proteins bound to DNA (Figure 1b). In the first step, the pipette approaches the surface. The electrophoretic force captures the tethered molecule detected by a conductance drop, stopping at 200 nm from the surface once the molecule is inside the nanopore (Figure 1b-1). Due to the molecule entering the pore, the conductance through the glass nanopore drops. Then, the controlled translocation initiates at the start position and the glass nanopore moves backwards with sub-nanometer precision by the closed-loop piezo (Figure 1b-2). The measured conductance through the nanopore can then be plotted as a function of distance along the molecule, and structural features along the DNA molecule can be identified (Figure 1b-3), until the end position (Figure 1b-4). The controlled translocation generated corresponds to a conductance-distance fingerprint that reveals structural features along the translocated molecule, in this case, a DNA-dCas9 complex (red plot in Figure 1b). After this, we can go to a different molecule at a different XY position or scan the same molecule again. We can even stop before reaching step 4, and measure the same region of the molecule multiple times without removing the molecule from the pore. As a proof-of-concept, we performed SICS mapping over a 40 x 40 μm^2 area generating 100 controlled translocation traces (10 x 10 array with 4 µm pitch), detecting dCas9 binding specificity along the DNA contour length (Figure 1b and SI Figure 1). This approach also allowed performing combined fluorescence microscopy and operating at a lower ionic strength, while taking advantage of the tunable size of the glass pores to translocate DNA-protein complexes (see Supplementary Figure 2).

Controlled translocations of molecular rulers

The key difference between our technique and traditional nanopore experiments is how the translocation speed is controlled. In conventional nanopore experiments, the speed of the translocation is determined by the electrophoretic force and the viscous drag of the molecules in the solution and the pore. Translocation speed depends on several factors, such as ionic strength, molecular charge, thermal fluctuations, transient analyte interactions with pore, bias voltage, and nanopore geometry. The result is a stochastic nature of the translocation process. This manifests in non-uniform dwell-time distribution between the detection of equally spaced motifs on a molecule such as a DNA ruler, see SI Figures 3 and 4. Free translocations generate conductance signals as a function of time with non-uniform translocation velocity[17,28]. In addition to stochastic effects influencing the translocation speed, the selection of which molecules are translocated is governed by stochastic factors.

In SICS, however, the molecule of interest is tethered to the surface and the electrophoretic force is countered by a reaction force on the tether, which prevents the molecule from fully translocating. Translocation is solely governed by the motion of the glass nanopore, which can be controlled accurately during the experiment. With the ability to deterministically control the velocity, the conductance traces are now a function of distance instead of time. Figure 1c (controlled translocation) shows the equidistant motif on the DNA ruler. This decouples important experimental parameters (ionic strength, bias voltage) and uncontrollable factors (such as nanopore geometry) from the translocation speed and detection bandwidth. We can, therefore, independently optimize experimental parameters to improve the detection limit.

To assess the benefits of SICS we used DNA rulers[28,29] to characterize the effect of translocation velocity on SNR, precision and repeatability. This DNA ruler is composed of a 7'228 base pair DNA strand (2'458 nm) and 6 markers of DNA dumbbell hairpins which are positioned at 1'032 base pairs intervals along the DNA contour (Figure 2a). Figure 2b shows the conductance-distance curve generated by SICS, revealing 6 markers. Controlled translocation with SICS allows decreasing the speed by more than 4 orders of magnitude compared with typical free translocations, leading to an increased SNR (Figure 2c). At the lowest velocity of 0.1 μm/s, the SNR (conductance amplitude of the ruler divided by the root-mean-square conductance noise of the baseline) measured was 152 ± 33 with an 8 nm glass nanopore radius (Figure 2d). This corresponds to an order of magnitude improvement of SNR compared with a free-translocation (>100 μm/s velocity). Figure 2e shows a location precision of 1% with controlled translocations, compared with 30% in free translocations with glass nanopores of the same pore size. SICS inherently has lateral control and can map out diverse molecules tethered on the surface (Figure 2f) or scan the same molecule again (Figure 2g). This spatial addressability allows us to multiplex the measurements to multiple molecular species. In free-translocation, differences in the detected amplitudes cannot be validated at the single molecule level due to the non-uniform translocation speed and limited transimpedance bandwidth (As shown in SI Figure 4). SICS method can identify rare structures and perform several translocations on the same molecule, rather than measuring 100 molecules with assumed identical structure by design. If the particular molecule shown in Figure 2g had been part of the 100 different molecules measured in Figure 2f, the misfolding event would have been lost in the averaging.

Spatial addressability and spatial multiplexing of single molecules

To take advantage of our SICS platform regarding spatial addressability, multiplexing and resolution assessment, we engineered dsDNA that contained single-stranded regions ("DNA gaps") of various sizes. We custom-designed four different DNA constructs (SI Figure 6) that were 8'750 base pairs in length (2'975 nm) and presented DNA gaps of 80, 40, 20, or 12 nucleotides, corresponding to lengths of 27.2, 13.6, 6.8, and 4.1 nm, respectively (Figure 3a). As a proof-of-principle for spatially multiplexed single molecules, we deposited the four different DNA gap constructs in an area of 5 mm×5 mm (Figure 3b). Within a single experiment, using the same glass nanopore, we detected and discriminated the four different DNA molecules. Figure 3c shows distinct conductance amplitudes (ΔGgap) for the different 80, 40, 20, and 12 nucleotides (nt) gaps. Figure 3d shows that the measured conductance amplitude of the 80 nt gap (ΔGgap) was half of the dsDNA conductance drop (ΔGdsDNA) as expected, and the measured ΔG(dsDNA/ssDNA) ratio was 2.06 ± 0.13 (SI Figure 7). For smaller gap sizes, the measured ΔGgap decreases due to the convolution effects of the pipette geometry with the molecule structure and surface charge. To obtain reliable measurements on the smaller gaps, multiple measurements are desirable.

We use the sub-molecular spatial addressability (position the glass nanopore along the single molecule) to scan the same molecular region multiple times, with tunable bias and bi-directional readings (SI Figure 8 and 9). Figure 3e shows the probability density map of 1000 readings on the same feature (80 nt DNA gap). Asymmetries or differences in the shape of probability density map plots, were more noticeable when smaller diameter pipettes were used and when a large number of curves were recorded for the same molecule. If only 100 curves were used for Figure 3e, the asymmetries would be less noticeable (SI Figure 10). By recording and averaging conductance-distance curves of the same feature, we decreased the RMS noise of the averaged signal from 11.2 pS to 0.4 pS, increasing the SNR 20 times compared with a single reading (SI Figure 11).

Moreover, multiple reads of the same feature decreased the measurement error, and obtained an average amplitude of 157.3 pS with a standard error of 0.05 pS (0.03 % error), see SI Figure 11. Thus, our method yielded an SNR of 394 on the DNA gap, corresponding to an improvement of two orders of magnitude compared to free translocations. By accessing specific regions of the DNA molecule and by averaging the conductance fingerprints, we reliably detected gaps as small as 12 nucleotides (4.1 nm) with high SNR. The conductance traces for smaller gap sizes (12 and 20 nucleotides) measured with different pipettes indicate that the dimension of glass nanopores strongly influences the detected conductance drop. Remarkably, we estimated that the pipette's radii below 10 nm hint at an ultimate detection capability down to single nucleotide gaps (SI Figure 12).

Single base gap detection in dsDNA

To have finer control over the gap size, we created a library of oligonucleotides complementary to the DNA gaps (gap adaptors shown in SI Table 1). As a proof-of-concept, we hybridized 79 nt single-stranded DNA (oligonucleotide) to complementary 80 nt DNA gap molecules (DNA gap template) and then deposited the non-hybridized 80 nt DNA gap template on the same area of the substrate (Figure 4a).. Within a single experiment and the same glass nanopore, we compared controlled translocations on the 80 nt gap template (Figure 4b - Top) and the 1 nt gap in the hybridized complex (Figure 4b - Bottom). Our results demonstrate the single nt gap detection of SICS, with an average gap amplitude detected of 31.2 pS for a glass nanopore of 7 nm radius. Furthermore, the hybridization does not have to happen before depositing but rather in situ after depositing the template (Figure 4c). We demonstrated in-situ hybridization of 19 nt oligo strand with a complementary 20 nt gap, and the subsequent successful detection of the single nucleotide

gap with an average gap amplitude detected of 16.9 pS for a glass nanopore of 8 nm radius (Figure 4d). This indicates potential applications in diagnostics, DNA data storage and data retrieval[30].

Conclusions

We achieved full control of the translocation speed providing precise spatial and temporal control of the single-molecule experiments, demonstrated in several biomolecule systems such as DNA-protein complexes, molecular rulers, DNA gaps, in-situ oligonucleotide hybridization, and hairpin formation. The translocation control with SICS allows reading the same molecule, or region of a molecule, thousands of times, as well as scanning an array of different types of molecules. This control is independent of experimental parameters (ionic strength, bias voltage) as well as uncontrollable factors (such as nanopore geometry), and it allows for independent optimization of experimental parameters to improve the detection limit, unlocking the use of nanopore sensing in applications that previously required sub-nanometer resolution. ~~For the first time,~~ It was possible to reproducibly scan selected areas of a molecule, thereby addressing specific molecular regions of interest with unprecedented resolution and throughput. We achieved 100’000 readings per experiment and a scanning rate of 4 readings/s on a series of different molecules, each translocated multiple times. The ability to perform experiments with different molecular species within one experiment (see Figure 3b), drastically increases the experimental throughput and permits accurate comparison of the results given the identical experimental conditions (same glass nanopore, velocities, and buffer conditions). Besides enabling more detailed biophysical studies, this addressability enables new conceptual approaches to multiplexed diagnostics (multiple analytes on one DNA template) or DNA data storage, where the sample area could be spatially divided into sectors and folders, with the data stored in individual molecules acting as files.

In principle, SICS is able to detect any substrate-conjugated molecule; it has the potential to detect DNA and RNA at very low concentrations. In a diagnostic setting, the main factors determining its concentration detection limit are the efficiency of conjugate binding, the binding kinetics, and the capture efficiency. The demonstrations presented here constitute a fraction of DNA-based systems, and the full extent of molecules and biopolymers that SICS can be applied to are yet to be explored.

Currently, we used glass capillaries shrunken down with SEM to nanopore size. Fabricating these glass nanopores in a reproducible way remains a challenging task. It offers, however, the possibility to tune the nanopore size depending on the application. Whereas we preferred smaller nanopores for our DNA template-based (DNA rulers, DNA gaps) experiments, DNA/protein complexes often require bigger pores. The conical shape of the glass nanopores intrinsically limits the axial resolution of our measurements. Nevertheless, through the drastic increase of SNR, we could detect down to single nucleotide gaps in dsDNA. Additionally, SICS measurements could benefit from the fact that our SICS setup is integrated with a state-of-the-art optical microscope, enabling Förster resonance energy transfer (FRET)[31], single-molecule localization microscopy (SMLM)[32] and DNA-PAINT (DNA-based Point Accumulation for Imaging in Nanoscale Topography)[33] experiments.

Compared to other nanopore detection techniques, glass nanopores are more difficult to parallelize. This drawback, however, is partially mitigated by the ability to do spatial multiplexing, meaning that one glass nanopore could probe thousands of molecules arranged on the surface. The spatial multiplexing combined with the sub-nanometer resolution could be used in conjunction with micro-array technologies to enable screening of DNA, improving point of care devices, or enabling

high-density, addressable DNA data storage. The basis of SICS, the mechanical control of the translocation, could also be realized using solid-state nanopores in MEMS devices.

Integrating biological nanopores into the opening of the glass capillary[34] could combine the benefits of biological nanopores (high resolution and reproducibility) with the benefits of SICS (molecule independent speed control and multiple readings per molecule). We expect this to greatly enhance the suitability of nanopores for the sequencing of peptides and proteins.

Acknowledgements

S.M.L. and G.E.F. acknowledge the support from the Swiss Commission for Technology and Innovation under the grant CTI-18330.1., and the European Research Council under grant number ERC-2017-CoG; InCell. V.N., H.M., and A.R. acknowledge the support from the National Center of Competence in Research (NCCR) Bio-Inspired Materials and Max-Planck-EPFL Center of Molecular Nanoscience and Technology. K.C. and U.F.K. were funded by PoreDetect (ERC-2019-POC, 899538) and EarlyPore (ERC-2022-POC1, 101069324).

Author contributions

S.M.L. developed the SICS system and performed the SICS measurements. S.M.L. and V.N. performed data analysis with S.M.'s support. V.N. and H.M. prepared the single-molecule samples and fabricated nanocapillaries. G.P. and A.K. created DNA gap molecules. H.M. and S.F.M. created the oligonucleotides/DNA gap templates. K.C. and U.K. created DNA rulers and provided free translocation data. S.M.L. and B.D. built the original SICM setup used in this work. A.R., G.E.F., S.M.L. and V.N. designed experiments with input from all the authors. A.R. conceived the method. G.E.F. and A.R. supervised the project. S.M.L., G.E.F., and A.R. wrote the manuscript with input from all the authors.

Competing interest declaration

A.R., G.E.F, S.M.L., and V.N. filed a patent application PCT/IB2022/055136, Nanopore-based scanning system and method.

Main Figures

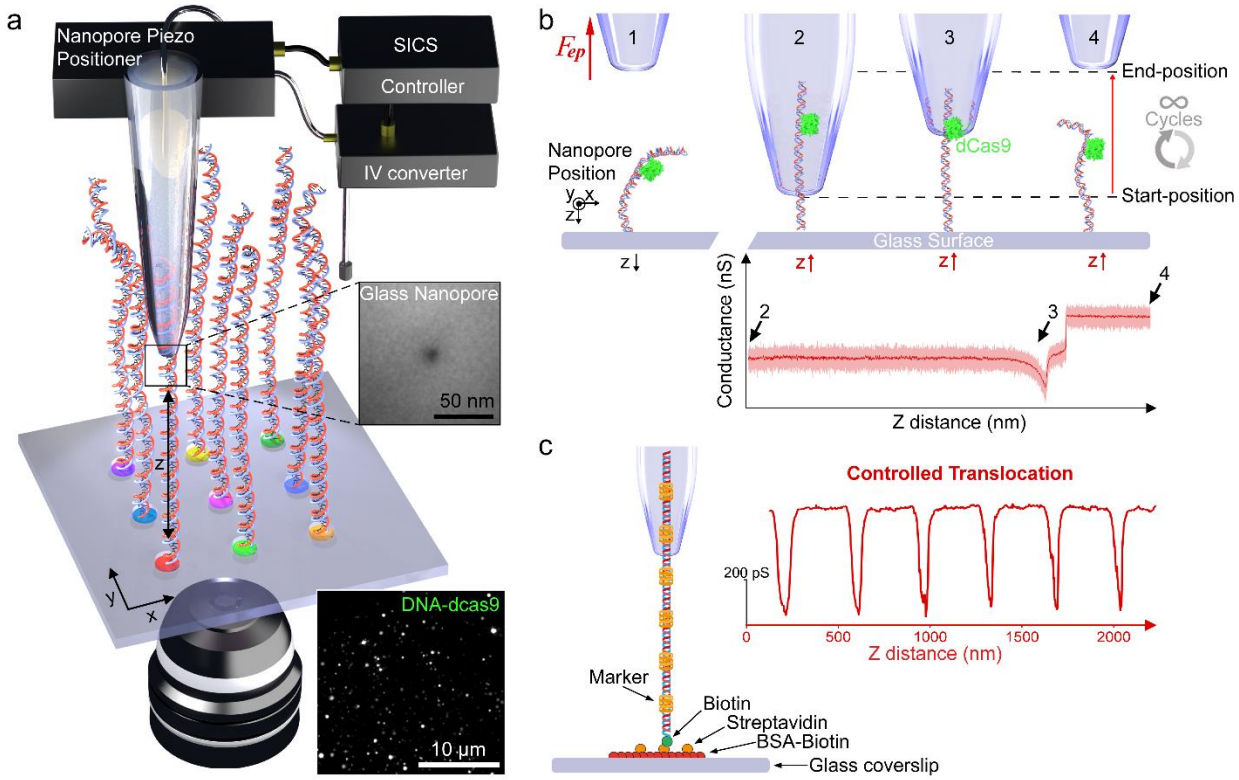

Figure 1. Controlled translocations of single molecules with nanopore-based scanning ion conductance spectroscopy (SICS). a) Schematics of the SICS system combined with fluorescence microscopy. Each color represents spatially multiplexed molecules deposited on the glass surface. **b)** Principle of SICS step-by-step, consisting in the molecule capture (1) followed by controlled translocation (2-4). (1): DNA shortly before capture in the nanopore by an electrophoretic force (F_{ep}) generated by a positive bias (50 – 600 mV). (2): Start-position of the controlled translocation along the DNA length. (3): Identification of a feature. (4): End-position of the controlled translocation followed by thousands of potential translocation cycles on the same molecule or mapping out different molecules upon XY displacement. The generated data corresponds to a conductance-distance curve revealing the DNA nanostructure, identifying a DNA-dCas9 complex in this case (red curve). 20 nm glass nanopore radius at 1 µm/s translocation velocity, 200 mV bias in 400 mM KCl, pH=7.4. Light red shows a conductance recording at 0.015 samples/nm and dark red trace shows the signal with an average window of 1 nm. **c)** SICS controlled translocation signature of a DNA ruler in optimal conditions with 8 nm glass nanopore radius at 1 µm/s translocation velocity, signal average window of 1 nm; 300 mV bias in 1 M KCl, pH=7.4. DNA molecules are tethered to a glass surface via biotin-streptavidin binding.

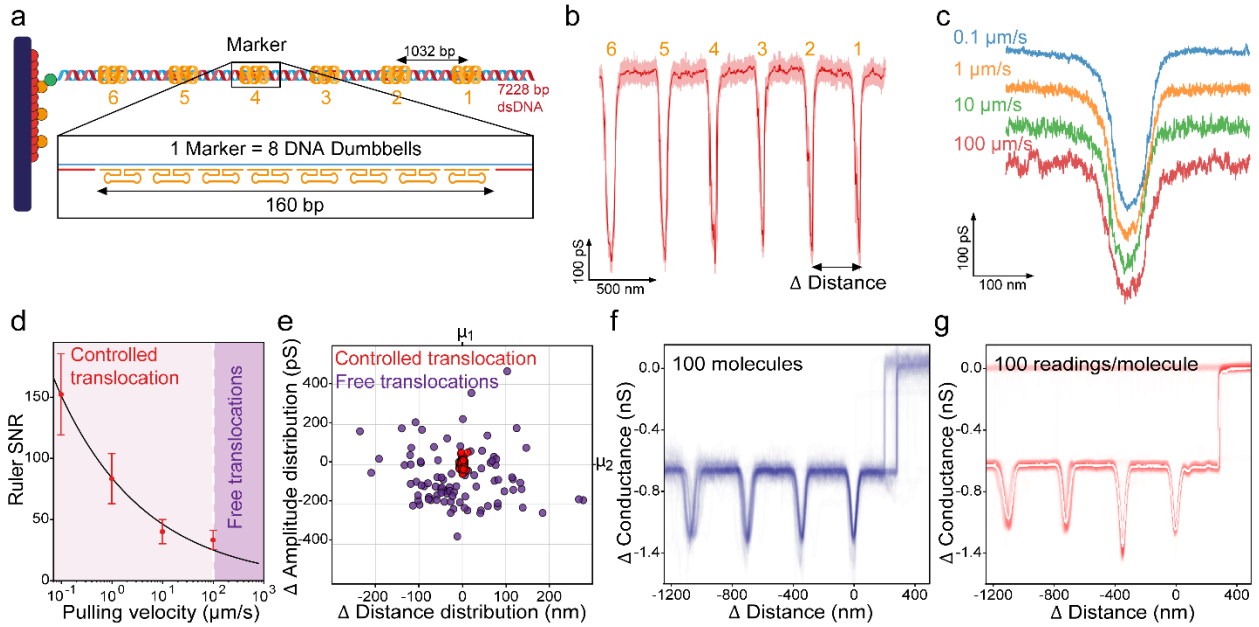

Figure 2. Controlled translocation of custom-designed DNA rulers increases SNR, precision, and accuracy. a) Design of the DNA ruler construct, composed of 7'228 base pairs with 6 markers containing DNA dumbbell hairpins separated by equal 1032 bp intervals. **b)** Controlled translocation of DNA ruler with 7 nm radius glass nanopore at 1 µm/s translocation velocity. Light red shows a conductance recording at 0.01 samples/nm and dark red trace shows the signal with an average window of 1 nm. Orange numbers above the trace indicate marker location along the DNA ruler. **c)** Controlled translocation at several velocities: 0.1 µm/s (blue), 1 µm/s (orange), 10 µm/s (green) and 100 µm/s (red); 8 nm radius glass nanopore, signal average window of 1 nm. **d)** SNR for the detection of markers at different translocation velocities. The error bars represent the standard deviation and the center is the mean SNR of all markers measured in several molecules (N = 12, 8, 12, and 8, for 0.1, 1, 10 and 100 µm/s respectively). **e)** Comparison of SICS translocations at 1 µm/s (red) with free translocations (purple) for glass nanopores of the same size (8 nm radius). The plot shows the distribution of the amplitude for marker 1 and the distance between markers 1 and 2 (Black arrows spacing in panel b), centered to the average distance (µ1) and average amplitude (µ2), N = 100. **f)** Overlay of controlled translocations for several molecules tethered on the surface, N = 100; Glass nanopores with radius of 8 nm were used at 1 µm/s translocation velocity, signal average window of 1 nm. Conductance traces were aligned to the first marker from the free-end. **g)** Overlay of controlled translocation of the same molecule (red) and their average (in white), N = 100; 8 nm radius glass nanopore at 1 µm/s translocation velocity, signal average window of 1 nm. All controlled translocation experiments were performed with 300 mV bias in 1 M KCl, pH=7.4.

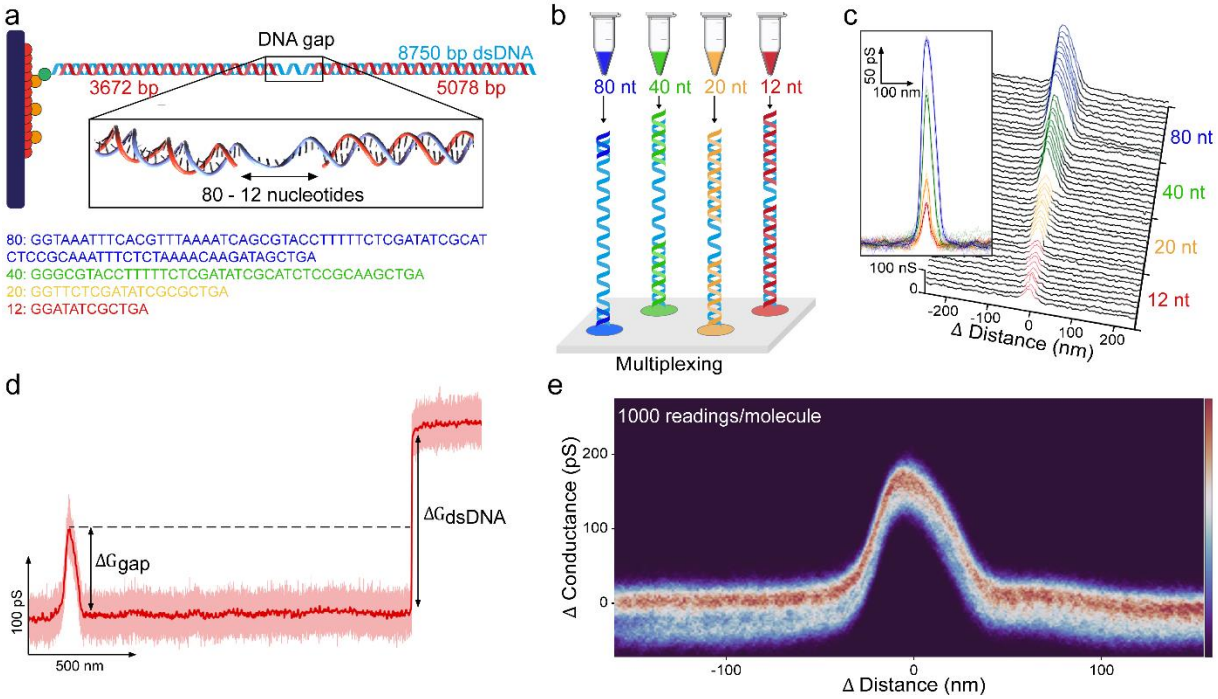

Figure 3. Spatial addressability of single-molecule translocations demonstrated on DNA gaps. a) Design of DNA gap construct composed of 8'750 base pairs and containing a central single-stranded region ("gap") of 4 different sizes: 80, 40, 20, or 12 nucleotides. **b)** Spatially multiplexed DNA gap molecules. **c)** Controlled translocation signals of DNA constructs with the different nucleotide gaps (N = 10 for each gap size molecule with the average in dark color) and corresponding waterfall plot. 8 nm glass nanopore radius at 1 μm/s translocation velocity, signal average window of 1 nm. **d)** Controlled translocation of the construct with an 80 nucleotide gap. The conductance amplitude (ΔGgap) of half the dsDNA translocation amplitude (ΔGdsDNA); 12 nm glass nanopore radius at 1 μm/s translocation velocity. Light red shows a conductance recording at 0.01 samples/nm and dark red trace shows the signal with an average window of 1 nm. **e)** Probability density map of 1000 readings in the same 80 nucleotide gap region, with a 10 nm glass nanopore radius at 1 μm/s translocation velocity, signal average window of 1 nm; the linear colormap represents the normalized probability of occurrence for a conductance value at a corresponding distance, 0 – 1 range. All the experiments were performed with 300 mV bias in 1 M KCl, pH=7.4.

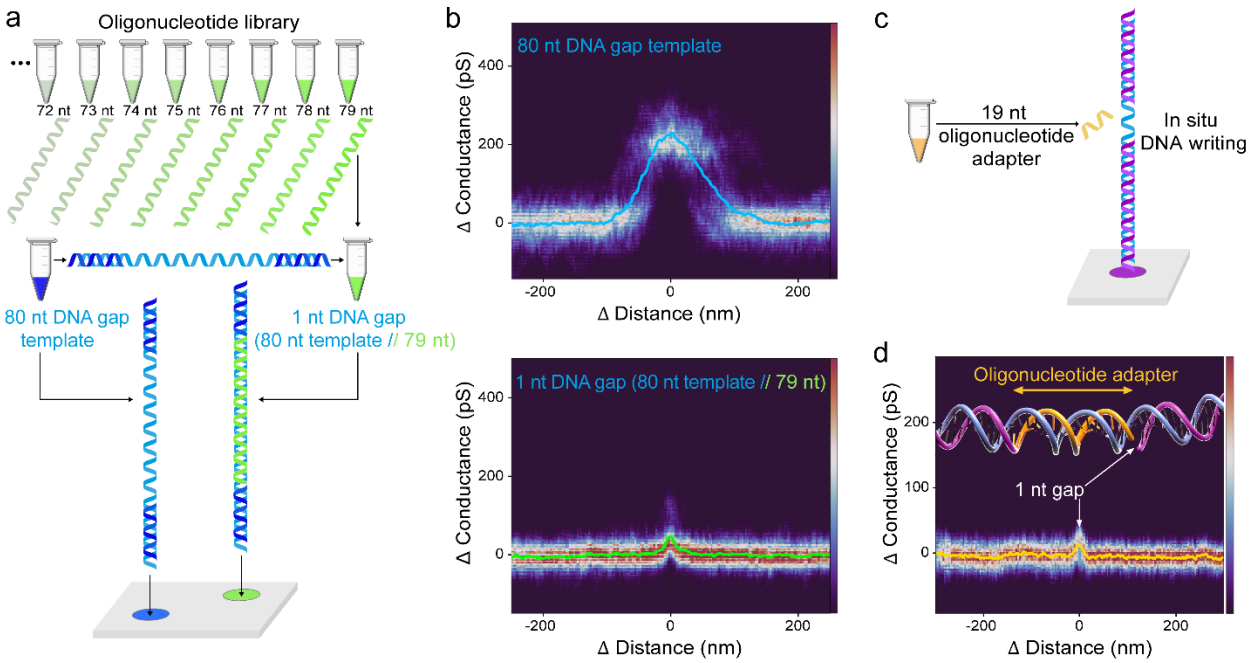

Figure 4. Detection of single nucleotide gaps with SICS. a) Strategy for creating shorter, variable gap sizes using multi nt gap template and complementary oligonucleotide library. **b)** Detection of an 80 nt DNA gap template (top) and a single nucleotide gap from a complementary 79 nt-long oligonucleotide hybridized to the gap (bottom), with a 7 nm glass nanopore radius at 1 µm/s translocation velocity, 0.01 samples/nm, N = 10; the linear colormap represents the normalized probability, 0 – 0.3 range. **c)** In situ hybridization concept for DNA writing, showing a gap template and addition of the complementary oligonucleotide (gap adaptor). **d)** A complementary 19 nt oligonucleotide was hybridized in situ on a 20 nt gap. The colormap represents the normalized probability. Reading of a 1 nt gap with 8 nm glass nanopore radius at 1 µm/s translocation velocity, 0.01 samples/nm, N = 10; the linear colormap represents the normalized probability, 0 – 0.5 range. All the experiments were performed with 300 mV bias in 1 M KCl, pH=7.4.

References

1. Branton, D. *et al.* The potential and challenges of nanopore sequencing. *Nature Biotechnology* **26**, 1146–1153 (2008).

2. Schneider, G. F. & Dekker, C. DNA sequencing with nanopores. *Nature Biotechnology* **30**, 326–328 (2012).

3. Brinkerhoff, H., Kang, A. S. W., Liu, J., Aksimentiev, A. & Dekker, C. Multiple rereads of single proteins at single-amino acid resolution using nanopores. *Science* **374**, 1509–1513 (2021).

4. Manrao, E. A. *et al.* Reading DNA at single-nucleotide resolution with a mutant MspA nanopore and phi29 DNA polymerase. *Nat Biotechnol* **30**, 349–353 (2012).

5. Derrington, I. M. *et al.* Subangstrom single-molecule measurements of motor proteins using a nanopore. *Nature Biotechnology* **33**, 1073–1075 (2015).

6. Fragasso, A., Schmid, S. & Dekker, C. Comparing Current Noise in Biological and Solid-State Nanopores. *ACS Nano* **14**, 1338–1349 (2020).

7. Li, J. *et al.* Ion-beam sculpting at nanometre length scales. *Nature* **412**, 166–169 (2001).

8. Storm, A., Chen, J., Ling, X., Zandbergen, H. & Dekker, C. Fabrication of solid-state nanopores with single-nanometre precision. *Nature Materials* **2**, 537–540 (2003).

9. Dekker, C. Solid-state nanopores. *Nanoscience And Technology: A Collection of Reviews from Nature Journals* 60–66 (2010).

10. Garaj, S. *et al.* Graphene as a subnanometre trans-electrode membrane. *Nature* **467**, 190–193 (2010).

11. Xue, L. *et al.* Solid-state nanopore sensors. *Nature Reviews Materials* **5**, 931–951 (2020).

12. Yusko, E. C. *et al.* Real-time shape approximation and fingerprinting of single proteins using a nanopore. *Nature Nanotechnology* **12**, 360–367 (2017).

13. Lu, B., Albertorio, F., Hoogerheide, D. P. & Golovchenko, J. A. Origins and consequences of velocity fluctuations during DNA passage through a nanopore. *Biophysical Journal* **101**, 70–79 (2011).

14. Plesa, C., Van Loo, N., Ketterer, P., Dietz, H. & Dekker, C. Velocity of DNA during

translocation through a solid-state nanopore. *Nano Letters* **15**, 732–737 (2015).

15. Rosenstein, J. K., Wanunu, M., Merchant, C. A., Drndic, M. & Shepard, K. L. Integrated nanopore sensing platform with sub-microsecond temporal resolution. *Nature Methods* **9**, 487–492 (2012).

16. Steinbock, L. J., Otto, O., Chimerel, C., Gornall, J. & Keyser, U. F. Detecting DNA folding with nanocapillaries. *Nano Letters* **10**, 2493–2497 (2010).

17. Bell, N. A. W., Chen, K., Ghosal, S., Ricci, M. & Keyser, U. F. Asymmetric dynamics of DNA entering and exiting a strongly confining nanopore. *Nat Commun* **8**, 380 (2017).

18. Steinbock, L. J., Bulushev, R. D., Krishnan, S., Raillon, C. & Radenovic, A. DNA translocation through low-noise glass nanopores. *ACS Nano* **7**, 11255–11262 (2013).

19. Aramesh, M. *et al.* Localized detection of ions and biomolecules with a force-controlled scanning nanopore microscope. *Nature Nanotechnology* **14**, 791–798 (2019).

20. Yuan, Z., Liu, Y., Dai, M., Yi, X. & Wang, C. Controlling DNA translocation through solid-state nanopores. *Nanoscale Research Letters* **15**, 1–9 (2020).

21. Rahman, M., Sampad, M. J. N., Hawkins, A. & Schmidt, H. Recent advances in integrated solid-state nanopore sensors. *Lab on a Chip* (2021).

22. Hansma, P. K., Drake, B., Marti, O., Gould, S. A. & Prater, C. B. The scanning ion-conductance microscope. *Science* **243**, 641–643 (1989).

23. Korchev, Y. E., Bashford, C. L., Milovanovic, M., Vodyanoy, I. & Lab, M. J. Scanning ion conductance microscopy of living cells. *Biophysical Journal* **73**, 653–658 (1997).

24. Novak, P. *et al.* Nanoscale live-cell imaging using hopping probe ion conductance microscopy. *Nature Methods* **6**, 279–281 (2009).

25. Leitao, S. M. *et al.* Time-Resolved Scanning Ion Conductance Microscopy for Three-Dimensional Tracking of Nanoscale Cell Surface Dynamics. *ACS Nano* **15**, 17613–17622 (2021).

26. Navikas, V. *et al.* High-throughput nanocapillary filling enabled by microwave radiation for scanning ion conductance microscopy imaging. *ACS Applied Nano Materials* **3**, 7829–7834 (2020).

27. Rief, M., Oesterhelt, F., Heymann, B. & Gaub, H. E. Single Molecule Force Spectroscopy on Polysaccharides by Atomic Force Microscopy. *Science* **275**, 1295–1297 (1997).

28. Chen, K. *et al.* Dynamics of driven polymer transport through a nanopore. *Nature Physics* **17**, 1043–1049 (2021).

29. Chen, K. *et al.* Digital data storage using DNA nanostructures and solid-state nanopores. *Nano Letters* **19**, 1210–1215 (2018).

30. Tabatabaei, S. K. *et al.* DNA punch cards for storing data on native DNA sequences via enzymatic nicking. *Nature Communications* **11**, 1–10 (2020).

31. Clegg, R. M. Fluorescence resonance energy transfer and nucleic acids. *Methods in Enzymology* **211**, 353–388 (1992).

32. Lelek, M. *et al.* Single-molecule localization microscopy. *Nature Reviews Methods Primers* **1**, 1–27 (2021).

33. Jungmann, R. *et al.* Single-molecule kinetics and super-resolution microscopy by fluorescence imaging of transient binding on DNA origami. *Nano Letters* **10**, 4756–4761 (2010).

34. Zhu, C. *et al.* Imaging with Ion Channels. *Analytical Chemistry* **93**, 5355–5359 (2021).

Methods

Experimental setup

SICS system and controlled translocation measurements

The SICS system is based on a high-speed scanning ion conductance microscope (HS-SICM) that we developed recently[1]. We modified our HS-SICM with the addition of a closed loop, long-range XYZ piezo scanner to precisely control the pipette motion and perform mapping curves in a similar way as done in AFM[2]. This enabled us to spatially select single molecules to translocate them at a controlled speed. In order to capture selected molecules, a bias is applied between two Ag/AgCl electrodes across the glass nanopore used in our system. When a positive bias is applied on the negatively charged DNA molecule tethered on the glass surface, the resulting force will pull the molecule through the nanopore, until the molecule is stretched between the surface and the nanopore. By moving the nanopore with respect to the surface, the conductance signature of the molecule inside the nanopore can be measured as a function of distance along the molecule, detecting specific features on the single molecule. The 3D nanopositioner used to translocate the molecules through the nanopore is a piezo-nanopositioning stage with 10 µm Z travel range and 100 µm X-Y travel range (P-733 Piezo NanoPositioner, Physik Instrumente), driven by a low-voltage piezo amplifier (E-500 Piezo Controller System, Physik Instrumente). The 3D nanopositioner was assembled in a custom-built micro translation stage, mounted atop an inverted Olympus IX71 microscope body. Thus, the SICS system enabled correlative fluorescence microscopy with a four-color (405 nm, 488 nm 561 nm, 647 nm) pigtailed Monolithic Laser Combiner (400B, Agilent Technologies), controlled by a custom-written LabVIEW software. An integrated sCMOS camera (Photometrics, Prime 95B) and Micromanager software were used to acquire images. The controlled translocation current signal was amplified by a transimpedance amplifier NF-SA-605F2 (100 MΩ gain, NF corporation) with a bandwidth of 10 kHz. The SICS controller was implemented in LabVIEW on a NI USB-7856R OEM R Series (National Instruments, Austin, TX, USA), to perform high-precision conductance-distance measurements and spatial mapping (conductance-volume mapping), similar to AFM force volume mapping[3], with a sampling rate up to 1 MHz. The controlled translocations were generated in 0.2 - 1 M KCl solution for bias ranging from 50 mV to 600 mV, while free translocations were generated in 1 M KCl and 4 M LiCl for bias ranging from 500 to 600 mV. Bias below 50 mV prevents the capture of the molecule, while bias above 600 mV leads to frequent contamination events and detachment of molecules.

Data processing and analysis

Controlled translocation curves were processed with a custom-written Python program which was used to automatically filter data, align different molecules, and calculate signal parameters. Single conductance-distance curves were averaged by a savitzky-golay filter with a window size of 1 nm. The root-mean-square conductance noise (RMS) measured corresponds to the square root of the average squared value of the conductance fluctuations from the mean conductance in a 20 nm range. To calculate the precision and compare controlled translocations with free translocations we used the relative standard deviation: RSD = (standard deviation ÷ average) × 100. Fluorescence image data analysis was performed using Fiji software[4] and AFM images were processed with Gwyddion software[5].

Statistics & Reproducibility

No statistical method was used to predetermine sample size.

Probe preparation

Fabrication and characterization of nanocapillaries

Nanocapillaries were fabricated using a CO2-laser puller (P-2000, Sutter Instrument). Quartz capillaries with 0.5 mm outer diameter and 0.2 mm inner diameter were bought from (Hilgenberg GmbH). Before the pulling process, all capillaries were cleaned with 99 % acetone, 99 % ethanol, MiliQ water (Millipore Corp) and again with 99 % ethanol by sonication in each solution for at least 10 min. After washing, nanocapillaries were dried in a desiccator for 1-2 h until they were completely dry and cleaned for 10 min in oxygen plasma. After the fabrication, nanocapillaries were characterized by a scanning electron microscope (Zeiss, Merlin). Nanocapillary diameters were confirmed using SEM, and as expected, under relatively high imaging current (400 pA), capillaries under 40 nm shrunk due to electron beam heating induced effects[6]. Diameters of all nanocapillaries were measured manually based on SEM images, using Fiji software[4]. See shrinking procedure and pore radius measurement in SI Figure 13.

Nanocapillary filling procedure

After SEM imaging, nanocapillaries were placed on the cover-glass with double-sided polyimide (Kapton) tape or a specially designed holder fabricated from PEEK plastic. Nanocapillaries were then cleaned with oxygen plasma (Femto A, Diener electronic GmbH) for 300 s at the maximum power setting. Immediately after, the nanocapillaries were immersed in a 400 mM or 1000 mM KCl solution and placed inside the desiccator connected to a vacuum pump. Nanocapillaries were kept under low-pressure (1-10 mbar) for 10 min to pre-fill them and avoid the formation of air bubbles in the thick end of the capillaries. Then they were imaged with an inverted brightfield microscope to confirm pre-filling. After, the nanocapillaries were placed inside a microwave oven (MW 1766 EASY WAVE, P = 700 W, λ= 12.23 cm). The highest power setting was always used. Microwave radiation was applied in heating cycles to heat the solution until its boiling point. The heating duration varied based on the volume and temperature of the solution. The first heating phase took (30-60 s), and subsequent heating phases were significantly shorter (5-10 s) due to the increased temperature of the capillary immersion solution. Heating was always stopped at the boiling point of a solution in order to minimize evaporation[6]. Short 10-20 s pauses were made in between heating steps to allow for the gas to dissolve into the solution. At least 3 heating cycles were performed to complete the filling of the nanocapillary batch[7]. After the procedure, capillaries were kept at 4 °C and the buffer was exchanged after a few hours to ensure the salt concentration was not affected by evaporation. For storage, nanocapillaries were kept at 4 °C in sealed chambers for up to one year.

Sample preparation

Lambda DNA preparation

10 kilobase long λ-DNA was prepared from full-length phage λ-DNA (New England BioLabs) by performing polymerase chain reaction (PCR) using one primer (Microsynth) with a biotin tag on the 5' end and the second one without biotin at the 3'. PCR was performed using a LongAmp DNA polymerase (New England BioLabs) following the protocol from the manufacturer. The reaction mixture was purified using PCR and a Gel Cleanup kit (Qiagen) from the agarose gel according to the protocol from the manufacturer. The length of the 10 kb λ-DNA product was verified with an agarose gel electrophoresis and the concentration was measured with a NanoDrop 1000 spectrometer.

gRNA preparation and immobilization

10kb long λ-DNA was screened for the presence of PAM motifs 5′X20NGG3′ and two targets separated by 5374 bp were selected. Single guide RNAs (gRNAs) were designed to be complementary to the 2 adjacent 20 bp PAM motifs previously selected on the λ-DNA. gRNAs were prepared by in vitro transcription of dsDNA templates carrying a T7 promoter sequence. Transcription templates were generated by PCR amplification of ssDNA templates containing the T7 binding site, 20 bp sequence complementary to the DNA target site, and sgRNA scaffold sequence using Phusion High-Fidelity DNA Polymerase (New England Biolabs). The gRNAs were synthesized by *in vitro* transcription using the MEGAshortscript T7 Transcription kit (Thermo Fisher) according to the manufacturer's conditions. The gRNAs

were treated with Turbo DNase (Thermo Fisher) and MEGAclear Transcription Clean-Up Kit (Thermo Fisher) was used for purification according to the protocol provided by the manufacturer. The concentration of purified gRNAs was measured with a NanoDrop 1000 spectrometer and the length and quality of the sgRNA were estimated by agarose gel electrophoresis. sgRNA samples were kept at -20 °C for a maximum time of 48h until further use.

dCas9-DNA complex formation

A commercially available inactive mutant of Cas9 nuclease (dCas9) with N-terminal SNAP-tag (EnGen Spy dCas9) was acquired from New England Biolabs. The protein was labeled with SNAP-Surface Alexa Fluor 647 labeling kit (New England Biolabs) according to the protocol provided by the manufacturer. The unreacted substrate was removed by the size exclusion column. Finally, fluorescently labeled dCas9 was incubated with gRNA in 1× NEBuffer 3.1 (New England Biolabs). 1 nM dCas9 was incubated with 10 nM gRNA for 30 min at 37 °C on an orbital shaker. 0.5 units of RNase inhibitors (Thermo Fisher) were used to prevent the degradation of RNA. After incubation, DNA was added at the final concentration of 50 pM and the mixture was further kept for 30 min at 37 °C on an orbital shaker. Schematics of the final constructs are shown in SI Figure 1a and dCas9-DNA binding controls were performed with AFM (SI Figure 14).

DNA ruler construct

DNA ruler constructs were prepared using previously published protocol[8]. The DNA ruler was synthesized by cutting circular 7249 base M13mp18 ssDNA (New England Biolabs) using the enzymes EcoRI and BamHI to form a linear ssDNA chain 7228 bases in length. The final scaffold was then purified and mixed in a 1:5 ratio with 212 oligonucleotides that formed a double-strand with six equidistant zones of dumbbell hairpins. The mixture is then annealed and purified. The final construct contains 6 markers with 8 dumbbells each. Markers are equally positioned in intervals of 1032 bp (See SI Figure 3).

DNA gap construct

DNA gap constructs were generated using modified 9 kb plasmids. In short, the pPIC9K plasmid (Invitrogen) was mutated using Q5 Site-Directed Mutagenesis (New England BioLabs) to insert two restriction sites specific for the nicking endonuclease Nt.BbvCI (New England BioLabs). Four plasmids were engineered with restriction cut sites that were 80, 40, 20, or 12 nt apart and that flanked an EcoRV restriction site. To generate a specific DNA gap fragment, the corresponding purified plasmid was first linearized by restriction digestion and biotin-labeled using Biotin-11-dUTP (ThermoFisher) and Klenow fragment (New England BioLabs). The DNA fragments were then digested with Nt.BbvCI to obtain single-strand breaks (nicks) and gapped by repeated (3x) heating cycles (90 °C, 60 sec; 60 °C, 10 min; 37 °C, 20 min) in the presence of a single-stranded competitor oligonucleotide (i.e. complementary to the DNA sequence comprised between the nicks)[9]. Finally, the construct was digested with EcoRV to eliminate ungapped fragments[10] analyzed on a 1 % agarose gel and purified (Monarch DNA gel extraction kit, New England BioLabs). The final dsDNA constructs were 8’750 base pairs long with biotin attached on one end, and a gap of 80, 40, 20, or 12 nucleotides (See Figure 3 and SI Figure 6). The sequence of the single-stranded stretches in the gap constructs were: 80 nt: GGTAAATTTCACGTTTAAAATCAGCGTACCTTTTTCTCGATATCGCATCTCCGCAAATTTCTCTAAAAC AAGATAGCTGA; 40 nt: GGGCGTACCTTTTTCTCGATATCGCATCTCCGCAAGCTGA; 20 nt: GGTTCTCGATATCGCGCTGA; 12 nt: GGATATCGCTGA. Occasionally we observed hairpins during SICS experiments in samples measured right after incubation at 4°C (See SI Figure 15).

Oligonucleotide-DNA gap template construct

In order to create gaps of shorter length, we created a library of complementary DNA oligos of different lengths that were hybridized on already existing dsDNA with a gap (See SI Table 1). In this way, we got gaps of smaller sizes that can be found in the table. We hybridized them by mixing the ~9 kb dsDNA gap templates (20, 40, 80) with the oligo (termed gap adaptor) at a 1:100 ratio, and placing it in a thermocycler with the following program: the sample was heated at 70 °C for 5 min and afterward ramped down 1 °C for 1 min per cycle, over 60 cycles.

Imaging chambers for DNA immobilization

The imaging chambers that are compatible with single-molecule fluorescence and single-molecule scanning ion conductance microscopy imaging were fabricated from high precision No. 1.5 borosilicate 25 mm coverslips (Marienfeld). Coverslips were cleaned with ethanol, then MiliQ water, dried with nitrogen flow, and cleaned with oxygen plasma (Femto A, Diener electronic GmbH) at maximum power for 660 s. After cleaning the open circular chamber made from a 1 mL pipette tip was glued on top with polydimethylsiloxane (PDMS), forming the final assembly. Fabricated chambers were kept in sealed petri-dishes until further use. For multiplexing, we made four small chambers (each of 5 µl volume) located on the same coverslip (see Figure 3). In the same way, adopting the robotic spotting methodology used in the preparation of microarrays[11], on a single 25 mm coverslip, one could accommodate more than 400 000 samples in the same buffer conditions.

Surface immobilization

100 µL of 1 mg/ml of BSA-Bt (Sigma-Aldrich) in PBS was incubated for at least 1 h in plasma-cleaned chambers to achieve the full glass surface coverage. Samples then were washed 10× with PBS by exchanging half of the solution, but without drying a surface. Samples then were incubated with 0.1 mg/ml of streptavidin (Sigma-Aldrich) for 1 h, followed by a 10× wash with PBS. Finally, 10-100 pM of DNA molecules were incubated for 1 h, followed by 10× wash with PBS or 3.1 NEBuffer. Samples were kept at 4 °C until use. The solution in the imaging chambers was exchanged by performing an additional 10× wash before imaging. The final imaging solutions are described in the imaging and SICS sections. We noticed that samples have not shown signs of degradation even after one year if kept at 4 °C in sealed petri-dishes that eliminates water evaporation.

Single-molecule fluorescence imaging

To optimize the surface density of DNA and to perform a control of dCas9 binding, samples were first imaged with a single molecule fluorescence microscope[12] (See SI Figure 16). For single-molecule imaging and to prevent photobleaching, a reductive/oxidative system (ROXS) based on glucose oxidase and catalase was used. Final buffer composition consisted of 2 mM TROLOX, 40 mM TRIS, 400 mM KCl, 1 % of glucose, 120 units/ml of glucose catalase, 15 units/ml. Buffer was filtered with a 200 nm filter. Imaging was performed in a sealed chamber to avoid oxygen exposure. All chemicals were acquired from (Sigma-Aldrich) unless stated otherwise.

Data availability statements

The data that support the plots Figs 1b and c, 2b-g, 3c-e, 4b and d in the manuscript are available via the research database Zenodo at https://doi.org/10.5281/zenodo.7834215.

Methods References

1. Leitao, S. M. *et al.* Time-Resolved Scanning Ion Conductance Microscopy for Three-Dimensional Tracking of Nanoscale Cell Surface Dynamics. *ACS Nano* **15**, 17613–17622 (2021).
2. Radmacher, M., Cleveland, J. P., Fritz, M., Hansma, H. G. & Hansma, P. K. Mapping interaction forces with the atomic force microscope. *Biophysical Journal* **66**, 2159–2165 (1994).
3. Rief, M., Oesterhelt, F., Heymann, B. & Gaub, H. E. Single Molecule Force Spectroscopy on Polysaccharides by Atomic Force Microscopy. *Science* **275**, 1295–1297 (1997).
4. Schindelin, J. *et al.* Fiji: an open-source platform for biological-image analysis. *Nature Methods* **9**, 676–682 (2012).
5. Nečas, D. & Klapetek, P. Gwyddion: an open-source software for SPM data analysis. *Open Physics* **10**, 181–188 (2012).
6. Steinbock, L. J., Bulushev, R. D., Krishnan, S., Raillon, C. & Radenovic, A. DNA translocation through low-noise glass nanopores. *ACS Nano* **7**, 11255–11262 (2013).
7. Navikas, V. *et al.* High-throughput nanocapillary filling enabled by microwave radiation for scanning ion conductance microscopy imaging. *ACS Applied Nano Materials* **3**, 7829–7834 (2020).
8. Bell, N. A. W., Chen, K., Ghosal, S., Ricci, M. & Keyser, U. F. Asymmetric dynamics of DNA entering and exiting a strongly confining nanopore. *Nat Commun* **8**, 380 (2017).
9. Wang, H. & Hays, J. B. Simple and rapid preparation of gapped plasmid DNA for incorporation of oligomers containing specific DNA lesions. *Molecular Biotechnology* **19**, 133–140 (2001).
10. Jozwiakowski, S. K. & Connolly, B. A. Plasmid-based lacZα assay for DNA polymerase fidelity: application to archaeal family-B DNA polymerase. *Nucleic Acids Research* **37**, e102–e102 (2009).
11. Auburn, R. P. *et al.* Robotic spotting of cDNA and oligonucleotide microarrays. *TRENDS in Biotechnology* **23**, 374–379 (2005).
12. Navikas, V. *et al.* Correlative 3D microscopy of single cells using super-resolution and scanning ion-conductance microscopy. *Nat Commun* **12**, 4565 (2021)..
13. Kowalczyk, S. W., Wells, D. B., Aksimentiev, A. & Dekker, C. Slowing down DNA translocation through a nanopore in lithium chloride. *Nano Letters* **12**, 1038–1044 (2012).